PROTEINS: Structure, Function, and Genetics 30:388–400 (1998)

Improved Protein Free Energy Calculation by More Accurate Treatment of Nonbonded Energy: Application to Chymotrypsin Inhibitor 2, V57A

Yuji Sugita and Akio Kitao*
Department of Chemistry, Graduate School of Science, Kyoto University, Japan

ABSTRACT **We developed a software package for improved free energy calculation, in which spherical solvent boundary potential, cell multipole method, and Nosé-Hoover equation are employed. The performance of the developed software package is demonstrated in the case of valine to alanine mutation of the 57th residue in chymotrypsin inhibitor 2. By using this package, we obtained results quantitatively comparable to experimental results. By the free energy component analysis, it is shown that leucine 51, arginine 65, arginine 67, and phenylalanine 69 residues contribute significantly to the total free energy shift, $\Delta\Delta G$. Among them, contribution from the hydrophilic arginine 67 residue, which is in close contact with the mutation site, is the largest. Structure around the mutation site is largely changed by the mutation. The structure change is caused mainly by two effects, hydrophobic interaction and short-range interaction along the sequence. Effects of Nosé-Hoover algorithm and Kirkwood reaction field are also discussed. Proteins 30:388–400, 1998.**

Key words: molecular dynamics; free energy perturbation; thermodynamics integration; spherical solvent boundary potential; cell multipole method; Nosé-Hoover equation; component analysis; chymotrypsin inhibitor 2

INTRODUCTION

Free energy calculation has now become a common tool for the study of proteins. The theory of free energy calculation is well established[1–4] and various computer program packages are available for scientists. However, attaining enough accuracy to be comparable with experimental results is still not a trivial problem for large systems containing a biopolymer. The insufficient treatment of molecular dynamics (MD) is one of the main causes of the insufficient accuracy of the free energy calculation. Our purposes in this article are the following: *(1)* to develop an integrated computer program for free energy calculation by assembling the best MD algorithms now available, and *(2)* to demonstrate that enough accuracy of free energy calculation of protein–water system is achieved by the developed program.

In order to attain purpose *(1)*, various simulation algorithms are examined. In the first place, boundary condition of the system is considered. Either spherical boundary condition or periodic boundary condition is usually used in the molecular dynamics of protein in explicit water molecules. In periodic boundary condition, the Ewald summation is commonly employed in which interactions among infinite number of replicas are calculated accurately.[5,6] This method is widely used in the simulation of liquid and a small solute in solution. The particle mesh Ewald method, the modified version of the Ewald summation, has been applied also for protein simulation in crystal environment.[7] Although good agreement of atomic fluctuation with experiment has been reported, this method can be applied only to neutral systems. In protein–water system, treatments of counterions are involved. Therefore, nonneutral subsystem is often employed in MD, although real system is always neutral. In order to achieve the generality of our program, spherical boundary condition is employed.

Among various spherical boundary potentials designed for molecular dynamics, spherical solvent boundary potential (SSBP)[8] satisfies the two conditions that are essential in free energy calculation: *(a)* Volume fluctuation of the sphere is allowed. *(b)* The space outside of the sphere is filled with dielectric continuum that has dielectric constant of liquid water. Condition *(a)* enables the isothermal isobaric ensemble and condition *(b)* enables the case where total charge of the system varies during free energy perturbation calculation.

Even with SSBP, the protein–water system still contains thousands of explicit atoms or more. Various algorithms have been proposed to calculate the

Contract grant sponsor: Ministry of Education, Science and Culture, Japan.
*Correspondence to: Dr. Akio Kitao, Department of Chemistry, Graduate School of Science, Kyoto University, Kyoto 606-01, Japan.
E-mail: kitao@qchem.kuchem.kyoto-u.ac.jp
Received 9 June 1997; Accepted 22 September 1997

electrostatic interaction among a huge number of particles with high accuracy.[9–14] These algorithms share the same concepts, cell hierarchy, and multipole expansion. Space is divided into small cells, which is called the deepest cells in the cell multipole method (CMM).[11,12] Pairwise nonbonded interactions are directly calculated for the atom pairs that are located in the same and next-neighboring cells. In other cases, atom–atom interactions are replaced by the interactions between atom and multipole of the cell. The size of the cell is hierarchically enlarged according to the increase of the atom–cell distance. The order of interacting pairs in the direct calculation, N^2, decreases to N log N in these algorithms, where N is the number of atoms. The CMM has an additional advantage that explicit calculation of atom–cell distance is not necessary. We employ CMM in our calculation.

The method of Berendsen[15] is employed commonly in the MD of proteins to maintain the system temperature constant. However, it has been proved that Berendsen's method does not lead to the canonical distribution.[16] Nosé solved this problem of realizing the canonical distribution by introducing one extra degree of freedom.[17] This method involves variable time steps. Hoover improved the method by developing an equation,[16] commonly referred to as the Nosé-Hoover equation, which involves a more convenient constant time step. We have chosen the rigorous Nosé-Hoover algorithm in our program.

Free energy calculation is performed by a software package that uses the algorithms listed above. In such calculations, we are interested in division of free energy shift into components, for example, covalent energy term, Lennard-Jones energy term, and electrostatic energy term. Free energy can be decomposed also into residue terms, atom terms, and so on. Recently, several theories regarding the path dependence of the free energy components have been advanced.[18–24] There are two types of path dependence, *artificial path dependence*, caused by error, and λ *path dependence*, caused by the ways of changing coupling parameter λ. Artificial path dependence, for example, free energy hysteresis between forward and reverse calculations, should be reduced when accurate calculation is performed. Therefore the extent of the artificial path dependence indicates the quality of the free energy calculation. On the other hand, the free energy component is intrinsically λ path-dependent. We believe that free energy component analysis is significant when the λ path is thoughtfully chosen and clearly defined. We believe that decomposition of free energy shift into elements is equivalent to the understanding of the free energy shift.

In order to accomplish purpose *(2)*, free energy calculation is demonstrated as applied to chymotrypsin inhibitor 2 (CI2). We have carefully chosen a small protein whose denatured state is expected to have no specific structure. Recently, this molecule has become a popular target for the study of folding. CI2 is a single domain molecule consisting of 83 residues and folds as a single cooperative unit by the two-state kinetics.[25] Free energy shifts for various mutations have been determined experimentally.[26–28] CI2 has two hydrophobic cores, *hydrophobic major-core* and *hydrophobic minicore*. Hydrophobic major-core is buried, and hydrophobic minicore, formed by L51, V57, and F69, is partly exposed to solvent. Those three residues are located in the reactive loop. Among those residues, V57 is invariant in homologous proteins, whereas L51 and F69 are variable.[27] V57 is located in the middle of the reactive loop and forms hydrogen bonds with enzyme when serine protease–inhibitor complex is formed.[29] In this article, free energy shift caused by V57A mutation is calculated and decomposed into free energy terms by using the program we have developed. We propose a physical picture of V57A mutation by analyzing free-energy components.

METHOD

Molecular Dynamics to Improve Free Energy Calculation

In order to improve free energy calculation, molecular dynamics simulation is carried out by using the following algorithms. Spherical solvent boundary potential (SSBP)[8] is employed to realize spherical boundary condition. In order to fix the notation, SSBP energy terms are briefly described here. The interaction between the explicit molecules and the implicit outer solvent is embodied in the potential of mean force, spherical solvent boundary potential ΔW,

$$\Delta W = \Delta W_{\mathrm{hsr}} + \Delta W_{\mathrm{vdw}} + \Delta W_{\mathrm{elec}} \tag{1}$$

where ΔW_{hsr}, ΔW_{vdw}, and ΔW_{elec} are the cavity energy, the van der Waals energy, and the electrostatic energy, respectively. The cavity free energy ΔW_{hsr}, is a hard-sphere restriction potential, which is a work needed to insert a hard sphere in a bulk solvent,

$$\Delta W_{\mathrm{hsr}} = \mathrm{pV} + \sigma \mathrm{S} \tag{2}$$

where p and σ are the pressure and surface tension of the bulk water and and are the volume and surface area of the sphere, respectively. This term is important in order to realize a variable radius. The van der Waals free energy, ΔW_{vdw}, is a sum of the potential of mean force between the hard sphere and water oxygen atoms. This energy term confines water molecules within the sphere. The electrostatic charging free energy, ΔW_{elec}, is a Kirkwood reaction field energy,

$$\Delta W_{\mathrm{elec}} = -\frac{1}{2}\sum_{l,m}\frac{4\pi|\mathrm{Q}_{lm}|^2}{(2l+1)}\frac{\epsilon_{\mathrm{bulk}}-1}{\epsilon_{\mathrm{bulk}}+\mathrm{l}/(\mathrm{l}+1)}\frac{1}{\mathrm{R}^{2l+1}} \tag{3}$$

where Q_{lm}, ϵ_{bulk}, and R are the multipole moment produced by charge distribution inside the sphere, dielectric constant of bulk water, and the radius of the sphere. Additional angular potential is applied to the water molecules within a shell of 1 Å near the boundary. Unrealistic orientations of water molecules near the boundary, which are observed in the simulation performed without using angular potential, are corrected (see Beglov and Roux's paper[8] for more details), although the correction is not perfect.

We employ the CMM.[11,12] In the original CMM, multipole expansion is applied to both electrostatic energy and Lennard-Jones energy. However, due to the difference of treatment of the Lennard-Jones parameters, multipole expansion cannot be applied to Lennard-Jones energy in AMBER energy function.[30] [In AMBER energy function, Lennard-Jones parameters for the interaction between type i and type j atoms, ϵ_{ij} and R_{ij}, are determined by the combination rules, $\epsilon_{ij} = (\epsilon_i\epsilon_j)^{1/2}$ and $R_{ij} = (R_i + R_j)/2$. CMM is applicable to the energy function with the combination rules, $\epsilon_{ij} = (\epsilon_i\ \epsilon_j)^{1/2}$ and $R_{ij} = (R_i + R_j)^{1/2}$.] Since Lennard-Jones energy is a short-range function, CMM for Lennard-Jones energy is not necessary if a sufficiently large deepest-cell size is employed. In our calculation CMM is applied only to electrostatic energy and the edge length of 6 Å is employed as the size of the deepest cell. The level of cell hierarchy is four and multipole expansion up to quadropole is applied. In trial calculations we achieved the same level of accuracy as was shown in the original CMM. Costs of the CMM and SSBP in energy calculation are about 20% and 10% of the total energy calculation, respectively. Multipoles of the cells that include the mutation site are calculated for the two hamiltonians. Since we only have to consider the energy difference, additional computation cost of CMM calculation in FEP is about 10% of the total CMM calculation.

MD is performed in isothermal-isobaric ensemble. To achieve isothermal condition, Nosé-Hoover algorithm is introduced. Isobaric condition is realized by the Beglov-Roux SSBP.[8] Nosé-Hoover equation[16,17] is solved by the Gear predictor-corrector algorithm.[31] Water molecules are treated as a rigid body. The five-value predictor–corrector is used for rotational motion of water molecules. For other degrees of freedom the six-value predictor–corrector method is employed. In order to achieve good energy conservation, combination of Nosé-Hoover, Gear predictor–corrector, and rigid water molecules should be carried out with a relatively short time step. The time step of the MD, Δt, is 0.5 fs.

Free Energy Calculation

Although the theory of free energy calculation is well established in the references,[1–4] it is briefly described here in order to fix the notation. The difference of stability between wild-type and mutant is estimated by free energy calculation. The free energy difference between wild-type and mutant is calculated, considering a thermodynamics cycle,[32–36]

$$\begin{array}{ccc} & \overset{\Delta G_1}{\longrightarrow} & \\ W_N & & W_D \\ \Delta G_3 \downarrow & & \downarrow \Delta G_4 \\ M_N & & M_D \\ & \underset{\Delta G_2}{\longrightarrow} & \end{array} \qquad (4)$$

where W_N, W_D, M_N, and M_D represent wild-type protein in the native state, wild-type in the denatured state, mutant in the native state, and mutant in the denatured state, respectively. ΔG_1, ΔG_2, ΔG_3, and ΔG_4 are the free energy shifts from W_N to W_D, from M_N to M_D, from W_N to M_N, and from W_D to M_D, respectively. From the relation in (4), free energy difference, $\Delta\Delta G$, is estimated by free energy perturbation calculation by using the relation, $\Delta\Delta G = \Delta G_3 - \Delta G_4$. Hamiltonian H [λ] is introduced, corresponding to paths of W_N to M_N or W_D to M_D so that H [0] = H_W and H [1] = H_M, where H_W and H_M are the hamiltonian of the states W and M, respectively. The Gibbs free energy change from the state W to the state M, ΔG, in the free energy perturbation (FEP), can be given by

$$\Delta G = -kT \sum_i \ln \langle \exp [-\Delta H [\lambda_i]/kT] \rangle_{NPT(\lambda_i)} \qquad (5)$$

where $<\cdot\ \cdot\ \cdot>$ NPT (λi) represents isothermal-isobaric ensemble average by using the hamiltonian H [λ] and $\Delta H [\lambda_i] = H [\lambda_{i+1}] - H [\lambda_i]$. An alternative is the thermodynamics integration (TI) where is written as

$$\begin{aligned} \Delta G &= \int_0^1 (\partial G/\partial\lambda)_{P,T}\, d\lambda \\ &= \int_0^1 \langle \partial H [\lambda]/\partial\lambda \rangle_{NPT(\lambda)}\, d\lambda. \end{aligned} \qquad (6)$$

By using Equation (6), free energy decomposition can be done as follows:

$$\begin{aligned} \Delta G &= \Delta G_{cov} + \Delta G_{nonbd} + \Delta G_{RF} \\ &= \Delta G_{cov} + \Delta G_{LJ} + \Delta G_{el} + \Delta G_{RF} \end{aligned} \qquad (7)$$

where ΔG_{cov}, ΔG_{nonbd}, ΔG_{LJ}, ΔG_{el}, and ΔG_{RF}, are covalent, nonbonded, Lennard-Jones, electrostatic, and reaction field components, respectively. Within the three SSBP terms, only the reaction field term, ΔW_{elec} of Equation (3), produces free energy difference. The ΔG_{nonbd} can be decomposed into two terms,

$$\Delta G_{nonbd} = \Delta G_{pro\text{-}pro} + \Delta G_{pro\text{-}wat} \qquad (8)$$

$\Delta G_{pro\text{-}pro}$ and $\Delta G_{pro\text{-}wat}$ are free energy components originated from protein intramolecular interactions

and protein–water interactions, respectively. The ΔG_{nonbd} can be decomposed also into $\Delta G_{\text{atom i}}$ and $\Delta G_{\text{residue a}}$ in atomic and residual level, respectively as

$$\Delta G_{\text{nonbd}} = \sum_{i} \Delta G_{\text{atom i}} = \sum_{i} \left[\frac{1}{2} \sum_{j} \Delta G_{\text{atom pair ij}} \right], \quad (9)$$

$$\Delta G_{\text{nonbd}} = \sum_{\alpha} \Delta G_{\text{residue } \alpha} = \sum_{\alpha} \left[\sum_{\substack{\text{atoms i} \\ \text{in residue } \alpha}} \Delta G_{\text{atom i}} \right], \quad (10)$$

where $\Delta G_{\text{atom pair ij}}$ is a free energy component originated from nonbonded interaction between atoms *i* and *j*. According to the definition, $\Delta G_{\text{atom i}}$ and $\Delta G_{\text{residue a}}$ are interpreted as *atomic free energy difference* and *residual free energy difference*, respectively. Since component analysis is performed during the course of TI calculation, additional computational cost is negligible.

Model of the Denatured State

In the denatured state simulation, a short peptide consisting of five residues including the mutation site in the middle (peptide model of the denatured state) is adopted. We will first examine an approximation involved in this treatment. Protein residues in the denatured state are classified into two types, "pept" residues, which are included in the peptide model, "rest" residues, which are not included in the peptide model. The free energy difference of protein–water system, ΔG[protein], is decomposed into three terms,

$$\Delta G[\text{protein}] = \Delta G_{\text{wat-pept}} + \Delta G_{\text{rest-pept}} + \Delta G_{\text{pept-pept}}, \quad (11)$$

here $\Delta G_{\text{wat-pept}}$, $\Delta G_{\text{rest-pept}}$, and $\Delta G_{\text{pept-pept}}$ are free-energy differences caused by the interactions between water molecules and "pept" residues, between the "rest" residues and "pept" residues, and among "pept" residues, respectively. In the peptide–water system, which is employed for denatured state model, is given by

$$\Delta G[\text{peptide}] = \Delta G_{\text{wat-pept}} + \Delta G_{\text{pept-pept}}. \quad (12)$$

In the peptide denatured state model, it is assumed that $\Delta G_{\text{wat-pept}}$ in Equation (11) is equal to $\Delta G_{\text{wat-pept}}$ in Equation (12) and is negligibly small. This is approximately valid when "rest" residues are located sufficiently far from the "pept" residues. In the experiment of V57A, protein denaturation has been caused by denaturant GdmCl.[27] Since denatured state caused by GdmCl is generally believed to be entirely unfolded, it is highly probable that "rest–pept" distance is sufficiently long. In addition, if atomic fluctuations in the denatured state are very large, interactions between "rest" residues and "pept" residues will be canceled out on average. In this case it is expected that peptide model gives reasonable results. If this assumption is valid, the ΔG[peptide] value is mainly determined by the peptide structure. Extended structure is employed as an initial coordinate of denatured state *M*D. In the case of V57A, this treatment would be justified by the following two reasons: *(i)* Local structure in entirely unfolded state tends to be extended rather than compact. *(ii)* Mutation site, which is located in the middle of an extended-like loop in the native state, is expected to form an extended structure rather than a compact structure also in the denatured state. The validity of the extended peptide model for the denatured state is reexamined in the Discussion section.

Simulation Procedure

The CI2 crystal structure determined by McPhalen and coworkers[37] at 2.0 Å resolution is employed as an initial coordinate of the native-state simulation. The first 19 residues have not been included in either the crystallographic experiment[37] or in the free energy measurement by fluorescence experiment.[27] The same treatment is done in our calculation. The numbering of residues starts from 20 to 83. The positions of 64 water molecules have been determined by crystallography. These water molecules (crystal water molecules) are initially placed at the positions determined in the crystal. Then, additional 1,712 water molecules are placed around CI2 molecule to fill a sphere of 25 Å radius.

In the denatured state simulation, a short peptide of extended form, consisting of five residues including the mutation site in the middle, is adopted. The N and C termini are modified to an acetyl group (ACE) and —NH—CH_3 (NME) group, respectively. Therefore the initial peptide sequence is ACE–TIVTM–NME. The numbering of residues begins with 54 to 60. Then, 1,066 water molecules are placed around the peptide molecule to fill a sphere of 20 Å radius. Both in the native and in the denatured states there are roughly three or more layers of water molecules. AMBER potential energy function[30] and TIP3P water model[38] are employed.

The native-state system is equilibrated by the following procedure:

1. Energy minimization of 2,000 steps is carried out with a large value of constraint for restricting CI2 heavy atoms and crystal water molecules to the initial positions.
2. 50 ps MD is performed in order equilibrate the system to 300 K and 1 atm, by gradually relaxing the constraints.
3. 50 ps MD is performed without constraints. The denatured state system is equilibrated similarly.

The FEP is done by using the single topology model[4] and the double wide sampling.[39] The λ values of individual energy terms are changed equally at the same time. Free energy components are defined under this pathway. The MD simulation is performed with λ_i values in Equation (5) being 0.1, 0.3, 0.5, 0.7, and 0.9. At each λ_i, 5-ps data collection is done for the FEP calculation in Equation (5) following 5-ps equilibration. We checked that free energy difference at each λ_i value converged within 5 ps. Starting from the coordinate after the equilibration, a total of 50 ps forward calculation (valine to alanine) is performed, and another 50-ps reverse calculation (alanine to valine) follows. In the course of valine to alanine mutation, six H^{γ} atoms gradually change into dummy atoms DA, and two C^{γ} atoms into H^{β}, respectively. The minimum-energy bond length of DA–H^{β} is shortened up to 0.4 Å by using the GASP algorithm.[40] The TI calculation is carried out by similar procedure except that the minimum-energy bond length of DA–H^{β} is kept constant at the initial value.

All the MD/FEP/TI calculations are performed by a newly developed program package based on the framework of minimization/MD program PRESTO.[41] Subroutines for calculating SSBP were kindly provided by Professor Benoît Roux.

RESULTS

Errors Caused by Improper Treatments of Electrostatic Interactions

In this section we demonstrate the appropriateness of our treatment of electrostatic interactions as compared with results obtained by other methods. For this purpose we carry out simulations in the following three ways:

1. Improved free energy calculation performed with all the improvements described in the METHOD (IP).
2. Equivalence of IP except that simulation is done without Kirkwood reaction field energy in Equation (3) (WORF).
3. Simulation was carried out with nonbonded energy cutoff at 10 Å and without reaction field energy (CUT).

WORF corresponds to the frequently used system of a cluster in vacuum with the cluster consisting of a protein molecule surrounded by a few layers of water molecules. These three simulations are carried out independently by starting from the same initial structure.

In Figure 1, atomic root-mean-square deviations (RMSD) averaged over all the atoms in CI2 from the initial conformation are shown as a function of time. During the course of simulation, the RMSD in CUT simulation does not even show the sign of convergence to the equilibrium state. The RMSD in WORF is also seen to be slightly drifting. That in IP converges to a reasonable value. The free energy differences determined by FEP-IP, TI-IP, FEP-WORF, and FEP-CUT are shown in Table I. The value obtained by CUT simulation is the farthest from the experimental one, and its error is the largest among the four treatments. The error in CUT is mainly caused by the large RMSD shown in Figure 1. Both in IP and in WORF, values are in good agreement with experimental one. Error in IP is smaller than that in WORF. Judging from both RMSD in MD simulation and free energy difference, it is concluded that CUT simulation is not reliable. The difference between FEP-IP and TI-IP is mainly caused by the difference of the alchemic bonds mentioned in Method. When we examined the same treatments of the alchemic bonds in FEP-IP and TI-IP treatments in a calculation of a system involving human lysozyme (details to be reported by Y. Sugita, A. Kitao, and N. Go, manuscripts in preparation), we obtained a very good agreement of the values of $\Delta\Delta G$.

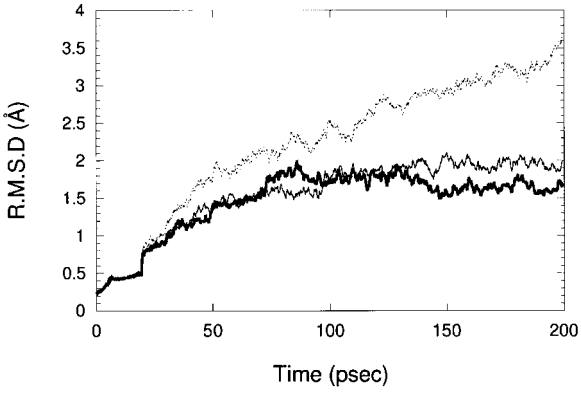

Fig. 1. Atomic root-mean-square deviation from the initial structure (RMSD) in IP, WORF, and CUT simulations during equilibration (first 100 ps) and forward free energy calculation (following 50 ps), and reverse free energy calculation (last 50 ps) are shown by *thick solid line, thin solid line,* and *dashed line*, respectively.

Structure Change Caused by Mutation

In Figure 2, instantaneous structures of CI2 in the native state are shown. We compare three structures, V1, A, and V2 structures, which represent structures averaged over the 5 ps duration, before the forward, after the forward, and after the reverse calculations, respectively. Significant deviations are seen mainly in the residues near the mutation site, G54, I56, V57, T58, and F69. Root-mean-square deviation (RMSD) of these residues between V1 and A, V1 and V2, and A and V2 of backbone atoms are, 1.01, 0.47, and 0.92 Å. In other words, the structures obtained after the reverse calculation are found to be similar to the structure before the forward calculation. This reversibility ensures the high accuracy of

TABLE I. Free Energy Differences (in kcal/mol) Between the Wild-Type and Mutant in the Native State, ΔG_N, and in the Denatured States, ΔG_D, and $\Delta\Delta G = \Delta G_N - \Delta G_D$, Obtained by Various Treatments

Treatment	Method of perturbation	ΔG_N	ΔG_D	$\Delta\Delta G$
IP*	TI	-2.99 ± 0.13	-4.17 ± 0.01	1.18 ± 0.13
	FEP	-3.32 ± 0.10	-4.99 ± 0.36	1.67 ± 0.37
WORF*	FEP	-4.47 ± 0.16	-5.99 ± 0.72	1.53 ± 0.74
CUT*	FEP	-5.41 ± 1.25	-5.13 ± 0.55	-0.29 ± 1.36
Experiment	—	—	—	1.47 ± 0.05

*The meaning of the error (values after ± in tables) in free energy calculation is the following. In ΔG, this value represents $|\Delta G(\text{forward}) - \Delta G(\text{reverse})|/2$. In $\Delta\Delta G$, this value represents the standard deviation of four values, ΔG_N(forward)–ΔG_D(forward), ΔG_N(forward)–ΔG_D(reverse), ΔG_N(reverse)–ΔG_D(forward), and ΔG_N(reverse)–ΔG_D(reverse).

the IP free energy calculation. The structure of the loop, vicinity of the mutation site, is largely changed by mutation in the native state. If two γ-methyl groups simply vanished without causing conformational change in protein, a large vacant space would be created between β-methyl group of alanine and surrounding atoms. The conformational change occurred in the way that the β-methyl group fills up this vacant space. In the denatured state, similar conformational changes occurred at the mutation site. This indicates that structural change occurs even in the absence of surrounding hydrophobic residues. In Figure 3 structure comparison of loop region between the native and the denatured states is shown. In the case of wild-type molecules, the peptide structure is similar to the loop structure in the native state, whereas the agreement in mutant is not good except in the mutation site. From these observations we conclude that the structure change in the native state during the mutation is caused by two effects, hydrophobic interaction and short-range interaction along the sequence.

Component Analysis of $\Delta\Delta G$ for V57A Mutation

Free-energy components are calculated by TI-IP. Decomposition of the free energy difference into covalent, Lennard-Jones, electrostatic, and reaction field terms [Eq. (7)] is shown in Table II. Although the Lennard-Jones term is a major part in ΔG, the dominant $\Delta\Delta G$ component is, due to cancellation, electrostatic rather than the Lennard-Jones term. Reaction field component is negligible in both ΔG and $\Delta\Delta G$. In Figure 4, the course of free energy change ΔG in TI, as well as components, are shown. Hysteresis of total ΔG and each component is quite small, being comparable to the best free energy calculations reported for small solutes. Thus, we have achieved the improvement of a computer program, which now produces quantitatively reliable results for systems containing a protein molecule. The covalent term is originated only from the changes of bond-length and bond-angle force fields within the mutated residue. Therefore residue–residue interactions are included only in the nonbonded terms.

As shown in Equation (8), the nonbonded terms are partitioned into protein–protein and protein–water interactions. As shown in Table III, protein–protein interaction is the major component both in ΔG_{nonbd} and in $\Delta\Delta G_{\text{nonbd}}$, although mutation site is partially exposed to the solvent. To examine the protein–protein interaction more in detail, the free-energy difference is decomposed into residues [Eq. (10)] as shown in Figure 5. The residues that are not shown in this figure do not contribute significantly. The residues that contribute considerably are L51, R65, R67, and F69 as well as the mutation site 57, its neighbors (I56 and T58), and the next neighbors (T55 and M59). The residues that are in contact with the mutation site are L51, T55, I56, T58, and R67. Due to the denatured state model, $\Delta\Delta G_{\text{nonbd}}$ components of L51, R65, R67 and F69 are only determined by the native state. The largest contribution to the total nonbonded component $\Delta\Delta G_{\text{nonbd}}$ comes from the mutation site and amounts to 64%. The L51 and F69, which form a hydrophobic minicore together with the mutation site, are destabilized mostly by the Lennard-Jones interaction. It should be noted that two arginine residues, R65 and R67, significantly contribute to $\Delta\Delta G$. In both residues, the Lennard-Jones and electrostatic contributions are almost equal. To further elucidate the interactions among these residues, free energy difference is decomposed into chemical groups. Chemical groups, whose nonbonded free energy components are significantly large, are shown in Table IV. The rather large contribution from the electrostatic components are notable. Those groups are in close contact with the mutation site (see Fig. 6).

DISCUSSION

Effect of Nosé-Hoover Algorithm

Before commenting on the CI2 results, let us briefly discuss the effect of Nosé-Hoover algorithm. Just for the purpose to examine this point, we have carried out the calculation of the difference of solvation free energy $\Delta\Delta G$ between ethane and methanol. The system consists of a solute and 132 water molecules. The method of calculation is equivalent to

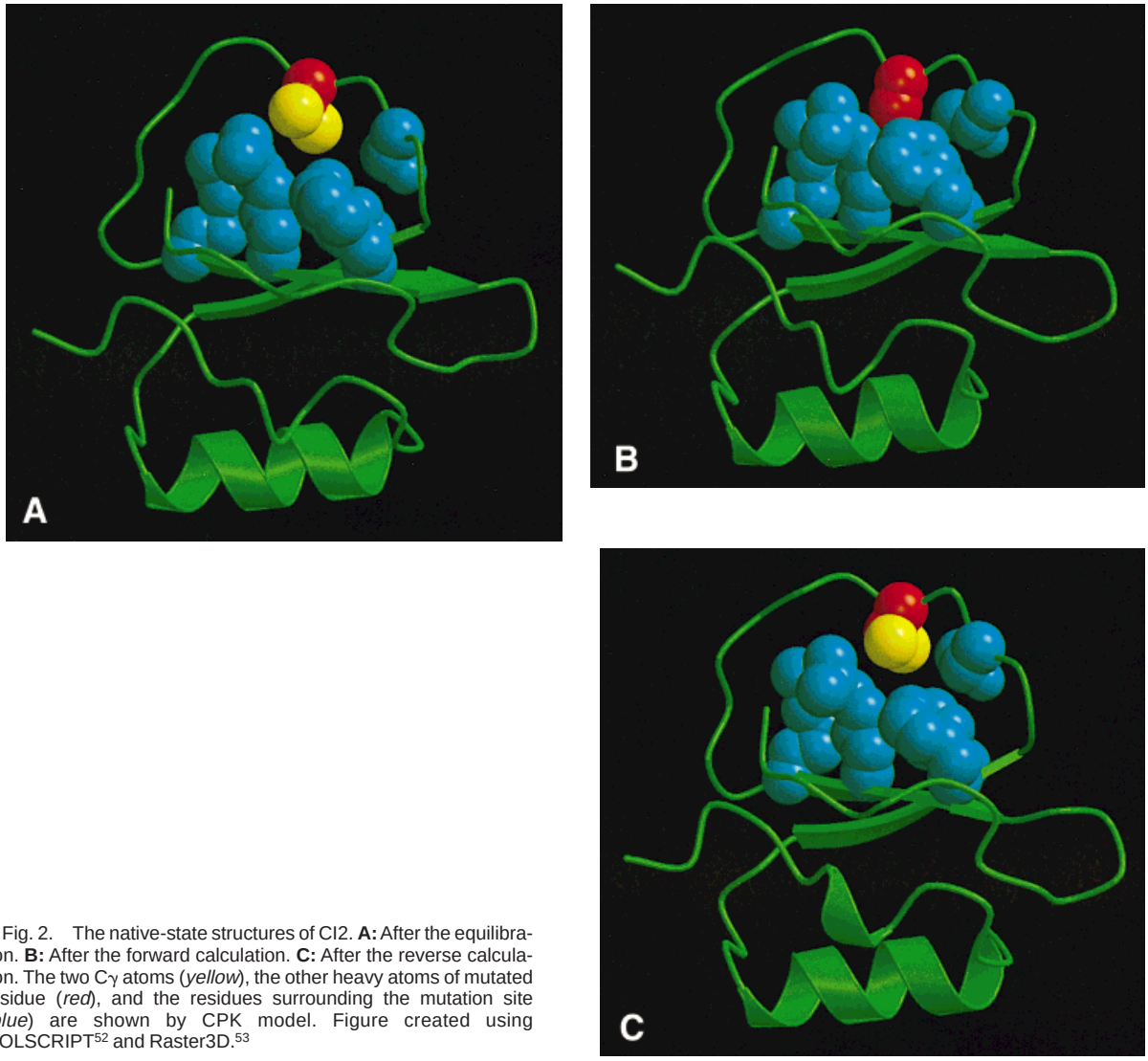

Fig. 2. The native-state structures of CI2. **A:** After the equilibration. **B:** After the forward calculation. **C:** After the reverse calculation. The two Cγ atoms (*yellow*), the other heavy atoms of mutated residue (*red*), and the residues surrounding the mutation site (*blue*) are shown by CPK model. Figure created using MOLSCRIPT[52] and Raster3D.[53]

IP calculation of CI2 except that nonbonded interactions are calculated directly without using CMM. As a control, another calculation is carried out by using SHAKE algorithm,[42] Berendsen's thermostat,[15] and leapfrog scheme. In the FEP calculation, free energy differences $\Delta\Delta G$ in IP and in the control are 7.5 ± 0.1 and 7.4 ± 0.1 kcal/mol, respectively. In this case, the IP results do not differ significantly from the control. Although we cannot jump to a general conclusion only from this calculation, it is probable that results obtained by Nosé-Hoover and Berendsen algorithms do not differ significantly. We nonetheless prefer to use the Nosé-Hoover algorithm because of its theoretical satisfactoriness.

Importance of Accurate Nonbonded Energy Calculation

Our results clearly show that cutoff approximations of electrostatic interaction should be avoided in free energy calculation. Although ΔG decays rapidly as a function of the distance from the mutation site as shown in Figure 7, the atomic free energy components at the usual cutoff distance are not negligible. Judging from preceding works[43] and our results, it is fair to conclude that quantitative estimate of free energy difference in the large systems is possible, only when no cutoff approximation is used. Although the introduction of reaction field does not produce notable change in the numerical value of the free energy, it is required to ensure statistical reversibility.

Effect of the Kirkwood Reaction Field Energy

As shown in Table I, the difference of $\Delta\Delta G$ between IP and WORF is not notable. This result can be clearly explained by considering the nature of the Kirkwood reaction field. In the V57A mutation, net charge in the sphere is invariant and change of the dipole and higher multipole would be small. This means that the change of the reaction field energy is

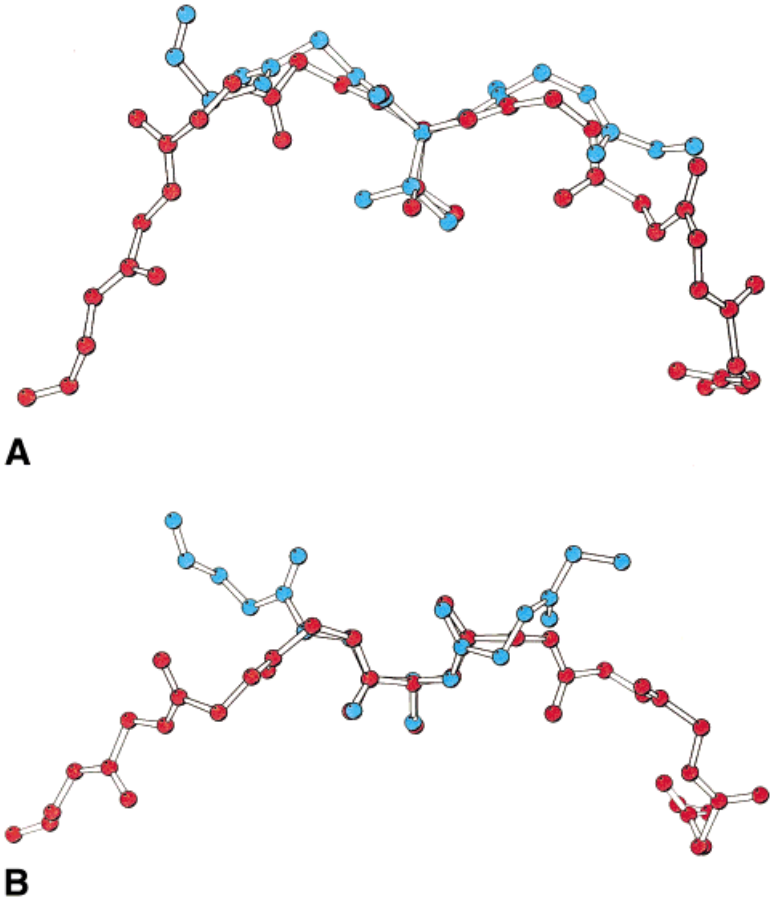

Fig. 3. Conformations around the mutation site in the native (*red*) and denatured (*blue*) states. **A:** After the equilibration. **B:** After the forward calculation. Figure created using MOLSCRIPT.[52]

very small against this mutation. However, in a case where net charge of the system changes, reaction field energy affects the free energy difference. To demonstrate this we have carried out a calculation of a difference of solvation free energy between Ne and Na^+. Both IP and WORF simulations are done by employing a series of different values of boundary sphere radius. Results are shown in Table V. Solvation free energies obtained by the IP simulations are found mostly independent of radius, whereas those by the WORF simulations are very much radius dependent and significantly underestimate the experimental value. In this case, where solute mutation site is placed at the center of the sphere, multipole moment is negligibly small. Therefore, the underestimation of free energy in the WORF simulation can be recovered roughly by adding Born energy, which is equivalent to the zeroth order ($l = 0$) of the Kirkwood reaction field energy in Equation (3).[44,45] In larger systems, effect of reaction field is smaller because Born energy is proportional to the inverse of the sphere radius. However, it still has a 5 kcal/mol shift in a case of the sphere with 30 Å radius. Therefore, consideration of the reaction field is crucial in the mutation of charged residue in proteins.

Two problems have been pointed out in the use of the reaction field.[46,47] In the course of the MD simulation the system may tend to produce a large dipole moment in the sphere so as to reduce the reaction field energy. As far as we tested, no notable difference is observed between IP and WORF calculations. Another problem is a response time of the reaction field. Real solvent molecules respond slowly to a certain event whereas the reaction field responds instantly. Ewald summation also has the same problem. Hence free energy is determined by not dynamics but by distribution, the instant response would not affect the free energy values significantly.

Here we point out that the use of Kirkwood reaction field energy should be carried out with care in the protein–water system. In the original SSBP, which has been designed and tested for the system consisting of small solute and water molecules, only one layer of water molecules around solute is sufficient to give reasonable free energy values. However, in the case of protein–water system, this treat-

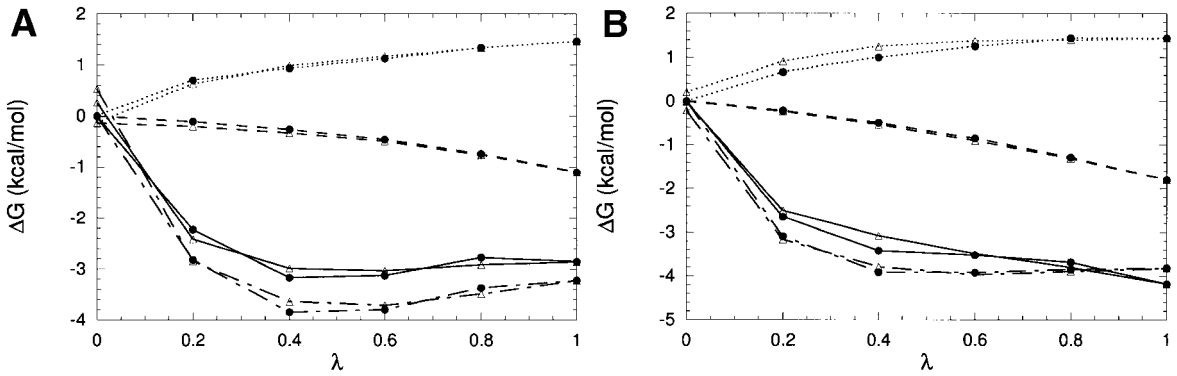

Fig. 4. The total free energy difference (*solid lines*), the covalent term (*dotted lines*), the Lennard-Jones term (*dot-dashed lines*), and electrostatic term (*dashed lines*). **A:** Native state. **B:** Denatured state. The data marked by *circles* and *triangles* represent the forward and reverse calculations, respectively.

TABLE II. Free Energy Components (in kcal/mol)*

	cov	LJ	el	RF
ΔG_N	1.53 ± 0.07	−3.49 ± 0.27	−1.03 ± 0.07	0.00 ± 0.00
ΔG_D	1.34 ± 0.10	−3.71 ± 0.10	−1.79 ± 0.01	0.00 ± 0.00
$\Delta\Delta G$	0.20 ± 0.12	0.22 ± 0.29	0.76 ± 0.07	0.00 ± 0.00

*cov, covalent; LJ, Lennard-Jones; el, electrostatic; RF, Kirkwood reaction field.

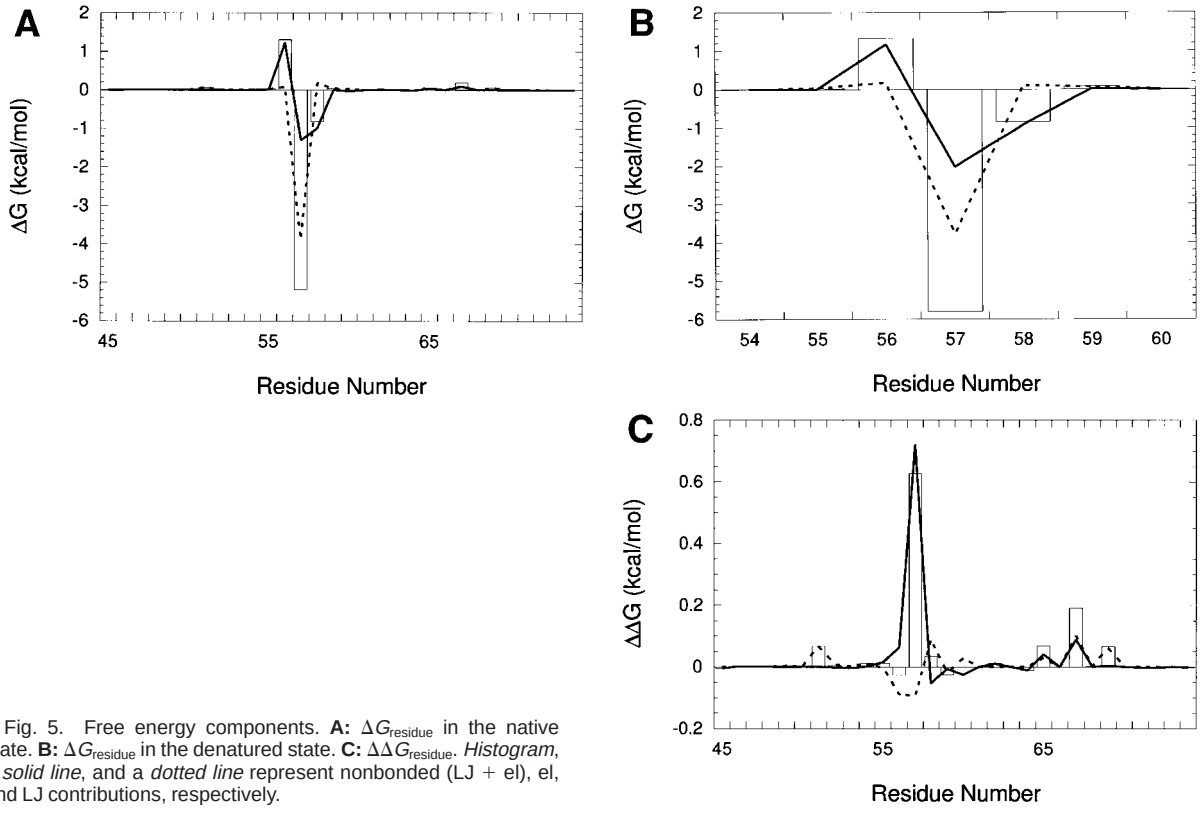

Fig. 5. Free energy components. **A:** $\Delta G_{residue}$ in the native state. **B:** $\Delta G_{residue}$ in the denatured state. **C:** $\Delta\Delta G_{residue}$. *Histogram*, a *solid line*, and a *dotted line* represent nonbonded (LJ + el), el, and LJ contributions, respectively.

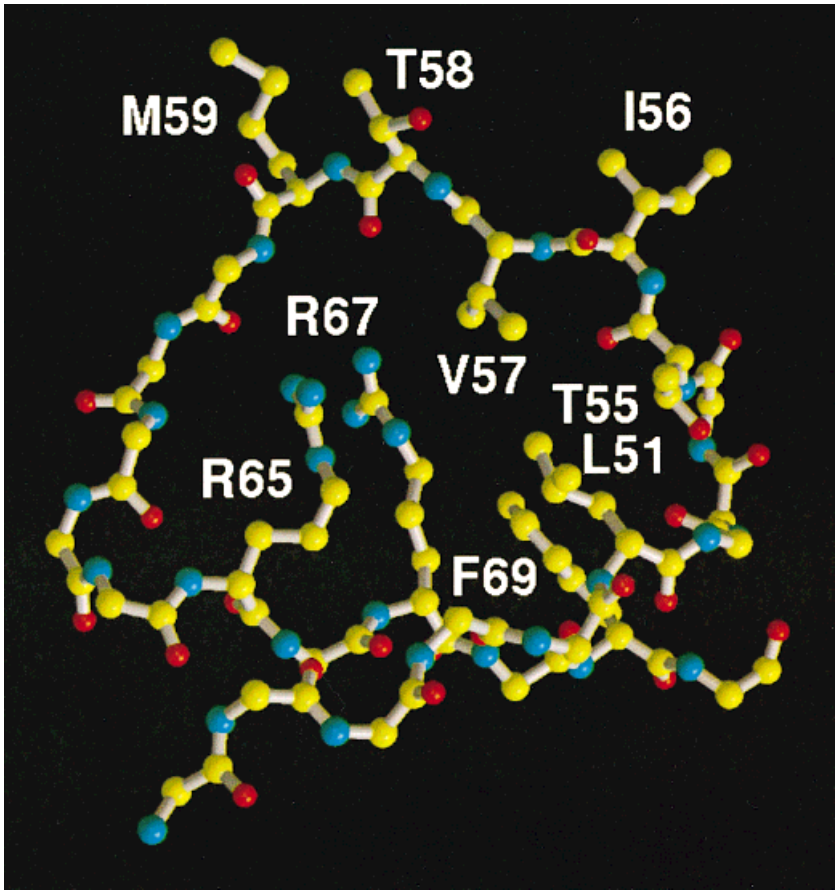

Fig. 6. Residues, whose contributions are significantly large, are shown. Figure created using MOLSCRIPT[52] and "Raster3D."[53]

TABLE III. Free Energy Contributions (in kcal/mol)

	Nonbonded	Protein–protein	Protein–water
ΔG_N	−4.52 ± 0.20	−3.87 ± 0.31	−0.66 ± 0.11
ΔG_D	−5.51 ± 0.11	−4.94 ± 0.18	−0.57 ± 0.07
$\Delta\Delta G$	0.98 ± 0.23	1.07 ± 0.39	−0.09 ± 0.13

ment is not recommended. If charged particle is located near the boundary, it is pulled to the boundary by Kirkwood reaction field. Charged side chains near the boundary might be pulled to the boundary, and structure of backbone atoms, which are connected to charged side chain, may also be changed largely. Therefore at least two or more layers of water molecules are necessary in protein–water system.

What We Learn From V57A Mutation

From the free energy component analysis, it is shown that R67 residue, which is in contact with one of the γ-methyl groups of V57, contributes significantly to the total free energy as well as L51 and F69 that form hydrophobic minicore together with V57. The importance of R67 has not been recognized, probably because the mutation involves only nonpolar moieties and this site has not been selected as a target of the mutation study.[26] The importance of residue R67 indicates that disappearing nonpolar

TABLE IV. Chemical Groups Whose Nonbonded Free Energy Components Are Significantly Large (Except the Mutated Residue) (in kcal/mol)*

Residue	Site	Group	LJ	el	nonbd
L51	Cδ1	—CH_3	0.000	0.029	0.030
T55	Cγ1	—CH_3	0.000	−0.063	−0.063
	C	$\diagdown$ C═O $\diagup$	0.012	0.014	0.026
I56	C	$\diagdown$ C═O $\diagup$	0.061	−0.138	−0.079
R67	Nϵ	—NH—	0.004	0.014	0.018
	Cζ	—C($\diagup$ $\diagdown$)	0.069	0.027	0.095

*Unit of free energy is kcal/mol.
LJ, Lennard-Jones; el, electrostatic; nonbd, nonbonded.

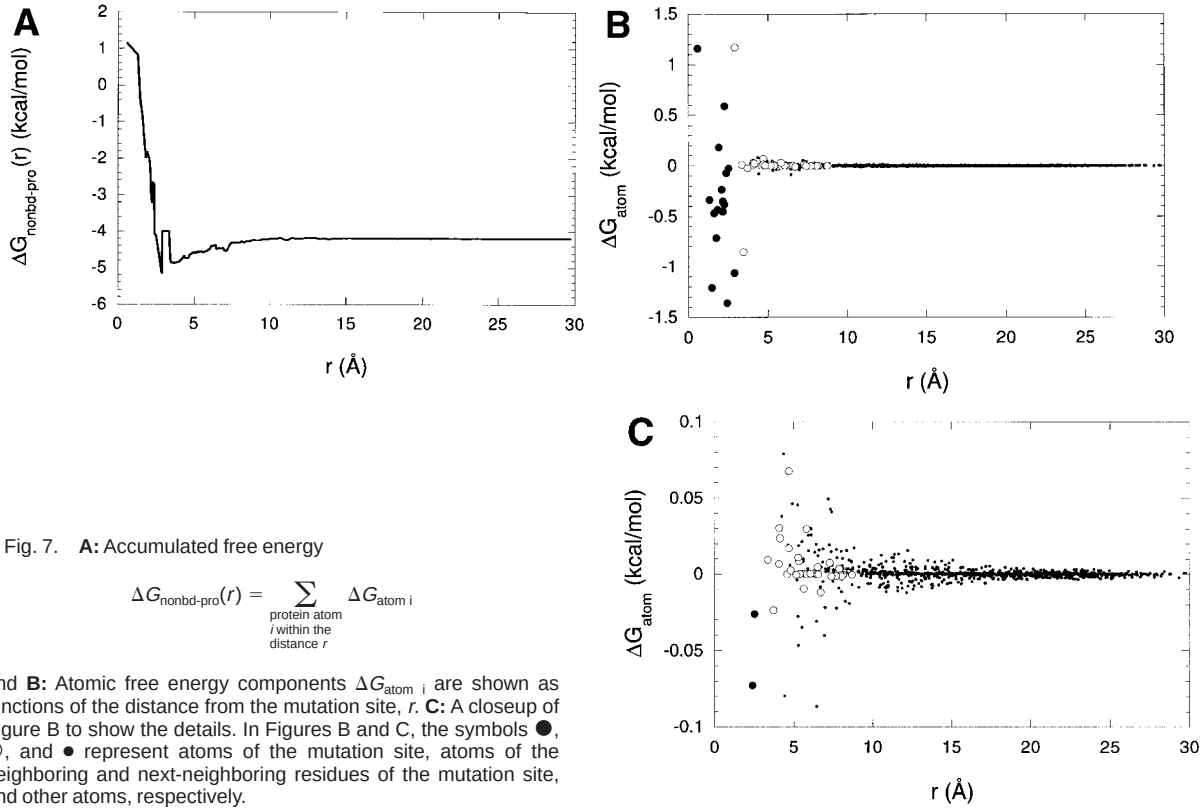

Fig. 7. **A:** Accumulated free energy

$$\Delta G_{\text{nonbd-pro}}(r) = \sum_{\substack{\text{protein atom } i \\ \text{within the} \\ \text{distance } r}} \Delta G_{\text{atom i}}$$

and **B:** Atomic free energy components $\Delta G_{\text{atom i}}$ are shown as functions of the distance from the mutation site, *r*. **C:** A closeup of Figure B to show the details. In Figures B and C, the symbols ●, ○, and • represent atoms of the mutation site, atoms of the neighboring and next-neighboring residues of the mutation site, and other atoms, respectively.

TABLE V. Differences of Solvation Free Energy Between Ne and Na^+, $\Delta G_{Ne \rightarrow Na^+}$ Calculated With and Without Kirkwood Reaction Field Energy (in kcal/mol) as a Function of the Sphere Radius*

Radius (Å)	No. water	IP	WORF	WORF + Born
6.0	28	−108.24 ± 0.07	−87.73 ± 1.00	−114.68
7.0	40	−108.99 ± 0.34	−88.87 ± 0.05	−114.29
8.0	67	−107.59 ± 0.07	−93.27 ± 0.64	−113.76
9.0	100	−109.18 ± 0.37	−94.61 ± 0.43	−112.83
10.0	135	−109.26 ± 0.90	−95.80 ± 0.42	−112.20

*Experimental value is −102.7 kcal/mol.

moieties have a nonnegligible free energy contribution from interaction with charged side chains. This would give some insights into the strategy of mutation.

As pointed out in the Introduction, V57 residue, which forms hydrogen bonds with enzyme by using main-chain polar atoms in the CI2–enzyme complex, is invariant among homologous proteins. In our calculation significant conformational change is observed in the V57A mutant. Judging from these results, it is suggested that V57 is invariant to maintain the specific loop structure necessary for inhibitor–enzyme recognition.

Justification of the Denatured State Model

As discussed in the Method section, it is assumed in the peptide denatured state model that $\Delta G_{\text{rest-pept}}$ is negligibly small. From the results shown in Figure 5, we can assess the effect of surrounding residues in the native state. Along the sequence, only the neighbor and next-neighbor residues have significant $\Delta\Delta G_{\text{residue a}}$ values. Other residues with large $\Delta\Delta G_{\text{residue a}}$ are located close to the mutation site. Although $\Delta G_{\text{atom i}}$ value in the native state shown in Figure 7 decays rapidly as a function of distance from the mutation site, the $\Delta G_{\text{atom i}}$ at certain distance, say 10 Å, is not negligibly small in the native state. In the denatured state, conformation should be much more flexible than in the native state. In this case it is expected that the $\Delta G_{\text{atom i}}$ decays more rapidly in the denatured state. Judging from the consideration in the Method section and in this section, it will be safe to say that the peptide model is a reasonable denatured state model in CI2 free energy calculation.

CONCLUSIONS

In this article, free energy calculation is improved by assembling the best molecular dynamics algorithms now available. In order to carry out molecular dynamics with high accuracy, spherical solvent boundary potential (SSBP), cell multipole method (CMM), and Nosé-Hoover equation are employed. The advantage of the present treatments is demonstrated in the case of valine to alanine mutation of the 57th residue in chymotrypsin inhibitor 2 (CI2). The results obtained by the present treatment (IP) are compared with those obtained by two treat-

ments, molecular dynamics without Kirkwood reaction field energy (WORF) and that further with cutoff approximation of nonbonded energy (CUT). IP is found to give results good enough to be compared quantitatively with the experimental results. Although difference of the calculated values by IP and WORF is relatively small, WORF simulation is seen to be slightly drifting even after 100 ps equilibration. The importance of the Kirkwood reaction field is demonstrated more pronouncedly in the case where total charge of the system changes during free-energy calculation. The difference of solvation free energy between Ne and Na^+ calculated by using Kirkwood reaction field energy is comparable to experimental value, whereas it is significantly underestimated when this energy is not include in the calculation.

Hystereses of free energy during the IP forward and reverse calculations are sufficiently small not only in the total free energy but also in their components. From the free energy component analysis, we found that nonbonded free energy difference $\Delta\Delta G_{nonbd}$ is mainly caused by protein–protein interaction rather than protein–water interaction. Among the residues that contribute significantly to the total free energy difference, the contribution from R67 is the largest. The importance of residue R67 indicates that disappearing nonpolar moieties have nonnegligible free-energy contribution from interaction with charged side chains.

Structure around the mutation site is largely changed by the mutation both in the native and denatured states. The structural change in the native state is caused by two effects, hydrophobic interaction and short-range interaction along the sequence. The V57 residue is invariant in homologous proteins and forms intermolecular hydrogen bonds when CI2 is bound to the enzyme. Judging from the computation results and amino acid invariance among homologous proteins, it is suggested that V57 should be invariant in order to maintain the specific loop structure necessary for binding.

Finally, we comment on the usefulness of the software package that we have developed. One of the fundamental problems in protein research is how protein native-state structures are stabilized. To understand this problem, various mutants have been created systematically and free energy shifts caused by the mutations have been measured extensively.[26,48–51] However, in considerable cases, effects of mutations on stability cannot be sufficiently explained only by experimental data. If these free energy shifts are decomposed into energy terms, effects of mutations are clearly explained. Since improved free energy calculation is achieved by the developed package, it is expected to become an essential tool for the understanding of protein stability.

ACKNOWLEDGMENTS

We thank Professor Nobuhiro Go for essential support of the research and research environment, and Professor Benoît Roux for providing us FORTRAN subroutines for the SSBP calculation. Computations were done at the Computer Centers of Kyoto University, Center for Promotion of Computational Science and Engineering, Computer Centers of the Institute for Molecular Science, and by CRAY J916 in our laboratory.

REFERENCES

1. Beveridge, B.L., DiCapua, F.M. Free energy via molecular simulation: Application to chemical and biomolecular systems. Annu. Rev. Biophys. Biophys. Chem. 18:431–92, 1989.
2. van Gunsteren, W.F., Mark, A.E. On the interpretation of biochemical data by molecular dynamics computer simulation. Eur. J. Biochem. 204:947–961, 1992.
3. Straatsma, T.P., McCammon, J.A. Computational alchemy. Annu. Rev. Phys. Chem. 43:407–435, 1992.
4. Kollman, P. Free energy calculations: Applications to chemical and biochemical phenomena. Chem. Rev. 93:2395–2417, 1993.
5. Ewald, P. Die Berechnung optischer und elektrostatischer Gitterpotentiale. Ann. Phys. 64:253–287, 1921.
6. Heyes, D.M. Electrostatic potentials and fields in infinite point charge lattices. J. Chem. Phys. 74:1924–1929, 1981.
7. York, D.M., Wlodawer, A., Pedersen, L.G., Darden, T.A. Atomic-level accuracy in simulations of large protein crystals. Proc. Natl. Acad. Sci. U.S.A. 91:8715–8718, 1994.
8. Beglov, D., Roux, B. Finite representation of an infinite bulk system: Solvent boundary potential for computer simulations. J. Chem. Phys. 100:9050–9063, 1994.
9. Greengard, L., Rokhlin, V. On the evaluation of electrostatic interactions in molecular modeling. Chem. Scripta 29A:139–144, 1989.
10. Greengard, L. Fast algorithms for classical physics. Science 265:909–914, 1994.
11. Ding, H.-Q., Karasawa, N., Goddard III, W.A. Atomic level simulations on million particles: The cell multipole method for Coulomb and London nonbond interactions. J. Chem. Phys. 97:4309–4315, 1992.
12. Mathiowetz, A.M., Jain, A., Karasawa, N., Goddard III, W.A. Protein simulations using techniques suitable for very large systems: The cell multipole method for nonbond interactions and the Newton-Euler inverse mass operator method for internal coordinate dynamics. Proteins 20:227–247, 1994.
13. Saito, M. Molecular dynamics simulations of proteins in water without the truncation of long-range coulomb interactions. Mol. Simul. 8:321–333, 1992.
14. Saito, M. Molecular dynamics simulations of proteins in solution: Artifacts caused by the cutoff approximation. J. Chem. Phys. 101:4055–4061, 1994.
15. Berendsen, H.J.C., Postma, J.P.M., van Gunsteren, W.F., DiNola, A., Haak, J.R. Molecular dynamics with coupling to an external bath. J. Chem. Phys. 81:3684–3690, 1984.
16. Hoover, W.G. Canonical dynamics: Equilibrium phase-space distributions. Phys. Rev. A 31:1695–1697, 1985.
17. Nosé , S. A molecular dynamics method for simulations in the canonical ensemble. Mol. Phys. 52:255–268, 1984.
18. Mark, A.E., van Gunsteren, W.F. Decomposition of the free energy of a system in terms of specific interactions implications for theoretical and experimental studies. J. Mol. Biol. 240:167–176, 1994.
19. Smith, P.E., van Gunsteren, W.F. When are free energy components meaningful? J. Phys. Chem. 98:2366–2379, 1994.
20. Boresch, S., Archontis, G., Karplus, M. Free energy simulations: The meaning of the individual contributions from a component analysis. Proteins 20:25–33, 1994.
21. Boresch, S., Karplus, M. The meaning of component analy-

sis: Decomposition of the free energy in terms of specific interaction. J. Mol. Biol. 254:801–807, 1995.
22. Zacharias, M., Straatsma, T.P. Path dependence of free energy components in thermodynamic integration. Mol. Simul. 14:417–423, 1995.
23. Brady, G.P., Sharp, K.A. Decomposition of interaction free energies in proteins and other complex systems. J. Mol. Biol. 254:77–85, 1995.
24. Brady, G.P., Szabo, A., Sharp, K.A. On the decomposition of free energies. J. Mol. Biol. 263:123–125, 1996.
25. Jackson, S.E., Fersht, A.R. Folding of chymotrypsin inhibitor 2. 1. Evidence for a two-state transition. Biochemistry 30:1428–1435, 1991.
26. Itzhaki, L.S., Otzen, D.E., Fersht, A.R. The structure of the transition state for folding of chymotrypsin inhibitor 2 analysed by protein engineering methods: Evidence for a nucleation-condensation mechanism for protein folding. J. Mol. Biol. 254:260–288, 1995.
27. Otzen, D.E., Rheinnecker, M., Fersht, A.R. Structural factors contributing to the hydrophobic effect: The partly exposed hydrophobic minicore in chymotrypsin inhibitor 2. Biochemistry 34:13051–13058, 1995.
28. Otzen, D.E., Fersht, A.R. Side-chain determinants of beta-sheet stability. Biochemistry 34:5718–5724, 1995.
29. McPhalen, C.A., James, M.N.G. Structural Comparison of two serine proteinase-protein inhibitor complexes: Eglin-C-subtilisin Carlsberg and CI-2-subtilisin novo. Biochemisry 27:6582–6598, 1988.
30. Weiner, S.J., Kollman, P.A., Nguyen, D.T., Case, D.A. An all atom force field for simulations of proteins and nucleic acids. J. Comput. Chem. 7:230–252, 1986.
31. Gear, C.W. "Numerical Initial Value Problems in Ordinally Differential Equations." Englewood Cliffs, NJ: Prentice-Hall, 1971.
32. Tidor, B., Karplus, M. Simulation analysis of the stability mutant R96H of T4 lysozyme. Biochemistry 30:3217–3228, 1991.
33. Sneddon, S.F., Tobias, D.J. The role of packing interactions in stabilizing folded proteins. Biochemistry 31:2842–2846, 1992.
34. Yun-yu, S., Mark, A.E., Cun-xin, W., Fuhua, H., Berendsen, H.J.C., van Gunsteren, W.F. Can the stability of protein mutants be predicted by free energy calculations? Protein Eng. 6:289–295, 1993.
35. Saito, M., Taminura, R. Relative melting temperatures of RNase HI mutant proteins from MD simulation/free energy calculations. Chem. Phys. Lett. 236:156–161, 1995.
36. Tanimura, R., Saito, M. Molecular dynamics/free energy perturbation studies of the thermostable V74I mutant of ribonuclease HI. Mol. Simul. 16:75–85, 1996.
37. McPhalen, C.A., James, M.N.G. Crystal and molecular structure of the serine proteinase inhibitor CI-2 form barley seeds. Biochemistry 26:261–269, 1987.
38. Jorgensen, W.L., Chandrasekhar, J., Madura, J.D., Impey, R.W., Klein, M.L. Comparison of simple poteintial functions for simulating liquid water. J. Chem. Phys. 79:926–935, 1983.
39. Reynolds, C.A., King, P.M., Richards, W.G. Free energy calculations in molecular biophysics. Mol. Phys. 76:251–275, 1992.
40. Severance, D.L., Essex, J.W., Jorgensen, W.L. Generalized alteration of structure and parameters: A new method for free-energy perturbations in systems containing flexible degrees of freedom. J. Comp. Chem. 16:311–327, 1994.
41. Morikami, K., Nakai, T., Kidera, A., Saito, M. PRESTO (PRotein Engineering SimulaTOr): A vectorized molecular mechanics program for biopolymers. Comput. Chem. 16: 243–248, 1992.
42. Ryckaert, J.P., Ciccotti, G., Berendsen, H.J.C. Numerical integration of the cartesian equations of motion of a system with constraints: Molecular dynamics of n-alkanes. J. Comp. Phys. 23:327–341, 1977.
43. Saito, M. Molecular dynamics/free energy study of a protein in solution with all degrees of freedom and long-range coulomb interactions. J. Phys. Chem. 99:17043–17048, 1995.
44. Kirkwood, J.G. The dielectric polarization of polar liquids. J. Chem. Phys. 7:911–919, 1939.
45. Straatsma, T.P., Berendsen, H.J.C. Free energy of ionic hydration: Analysis of a thermodynamic integration technique to evaluate free energy differences by molecular dynamics simulations. J. Chem. Phys. 89:5876–5886, 1988.
46. King, G., Warshel, A. A surface constrained all-atom solvent model for effective simulations of polar solutions. J. Chem. Phys. 91:3647–3661, 1989.
47. Nakamura, H. Roles of electrostatic interaction in proteins. Q. Rev. Biophys. 29:1–90, 1996.
48. Matthews, B.W. Structural and genetic analysis of protein stability. Annu. Rev. Biochem. 62:139–160, 1993.
49. Takano, K., Ogasahara, K., Kaneda, H., Yamagata, Y., Fjii, S., Kanaya, E., Kikuchi, M., Oobatake, M., Yutani, K. Contribution of hydrophobic residues to the stability of human lysozyme: Calorimetric studies and x-ray structural analysis of the five isoleucine to valine mutants. J. Mol. Biol. 254:62–76, 1995.
50. Funahashi, J., Takano, K., Ogasahara, K., Yamagata, Y., Yutani, K. The structure, stability, and folding process of amyloidogenic mutant human lysozyme. J. Biochem. 120: 1216–1223, 1996.
51. Takano, K., Yamagata, Y., Fujii, S., Yutani, K. Contribution of the hydrophobic effect to the stability of human lysozyme: Calorimetric studies and x-ray structural analyses of the nine valine to alanine mutants. Biochemistry 36:688–698, 1997.
52. Kraulis, P.J. MOLSCRIPT: A program to produce both detailed and schematic plots of protein structures. J. Appl. Crystallogr. 24:946–950, 1991.
53. Merrit, E.A., Murphy, M.E.P. Raster3D Version 20. A program for photorealistic molecular graphics. Acta Crystallogr. D50:869–873, 1994.